

The promotion and stabilization effects of surface nitrogen containing groups of CNT on cu-based nanoparticles in the oxidative carbonylation reaction

Guoqiang Zhang, Dan Zhao, Junfen Yan, Dongsen Jia, Huayan Zheng, Jie Mi, Zhong Li*

Key Laboratory of Coal Science and Technology of Ministry of Education and Shanxi Province, Institute of Coal chemical Engineering, Taiyuan University of Technology, Taiyuan, 030024, Shanxi, China

ARTICLE INFO

Keywords:

Nitrogen containing groups
Dispersion
Interaction
Promotion
Stabilization
Oxidative carbonylation

ABSTRACT

N-doped carbon nanotubes (NCNTs) with different contents of N were prepared by pre-oxidation and subsequent N-doping strategy and employed as the supports to fabricate Cu-based catalysts for oxidative carbonylation of methanol. The supports and their corresponding catalysts were characterized thoroughly by BET, XPS, XRD, H₂-TPR, TEM, N₂O chemisorption, CO-TPD, CH₃OH-TPD and ICP-OES measurements. It is found that the increase of oxygen containing groups generated by pre-oxidation can effectively improve the content of the nitrogen containing groups during the subsequent N-doping process. The nitrogen containing groups, especially the pyridine N groups, serving as the preferred anchoring site, significantly promotes the dispersion of Cu species. With the increased content of N from 0 to 5.2%, the dispersion of Cu species increases from 11.0 to 21.6% and the space time yield of DMC increases from 150.5 to 1789.6 mg g⁻¹h⁻¹. Moreover, the incorporation of nitrogen containing groups enhances the interaction between Cu species and CNT support, which suppresses the auto-reduction of Cu²⁺ to Cu⁺ and Cu⁰, while improves the anti-agglomeration, anti-oxidation and anti-leaching properties of Cu species. From the perspective of stability, the space time yield of DMC for Cu/CNT decreases from 150.5 to 86.9 mg g⁻¹h⁻¹ after four consecutive runs, while that of Cu/NCNT200 slightly decreases from 1789.6 to 1557.9 mg g⁻¹h⁻¹, and the declined degrees are 42.3% and 12.9%, respectively. The superior dispersion, anti-agglomeration, anti-oxidation and anti-leaching properties of Cu species as well as the promotion effect of pyridine N groups are contributed to the increased activity and stability of the Cu/NCNT200 catalyst.

1. Introduction

With the shortage of nature resources and pressure from environment issues, the production of green chemicals is gaining momentum in recent years, which demands us to develop green catalysts as well as eco-friendly and efficient synthetic routes. Dimethyl carbonate (DMC), an environmentally benign chemical, has been widely applied in the organic synthesis, as electrolytes in lithium ion batteries, and the prospective fuel additive, because of its low toxicity and bioaccumulation as well as excellent biodegradability, solubility and reactivity [1,2]. Among many synthesis routes, the oxidative carbonylation of methanol to DMC (2CH₃OH + CO + 1/2O₂ → (CH₃O)₂CO + H₂O) is considered as a promising approach due to its less environmental impact, preferable thermodynamics and high atom utilization rate [3–5].

The carbon supported CuCl, CuCl₂ and CuCl₂-PdCl₂ catalysts show high initial activity and selectivity, however, the Cl⁻ is easily eluted

during the reaction process, which subsequently results in deactivation of the catalysts, corrosion of equipment and also pollution of the environment [6–8]. Moreover, HCl is needed to supplement in the industrial production process to retard the deactivation of catalysts, which inevitably increases the security risks. Considering this, great attention has been paid to develop Cl⁻ free Cu-based catalysts.

The carbon supported Cu and CuO_x catalysts exhibit the catalytic activities comparable with that of Cl-containing ones and are considered as the “green” catalysts [9]. It is reported that the catalytic activities of Cu and Cu₂O are better than that of CuO, therefore, great efforts have been made to improve the content or the dispersion of Cu and Cu₂O [10–12]. Generally, the precursors of the catalysts firstly decompose and form CuO, which is subsequently reduced to Cu and Cu₂O by carbon supports [13,14]. The increase of calcination temperature can promote the reduction of CuO to Cu₂O or Cu, however, high calcination temperature leads to the decrease of dispersion and

* Corresponding author at: No. 79 Yingze West street, Taiyuan, 030024, China.
E-mail address: lizhong@tyut.edu.cn (Z. Li).

<https://doi.org/10.1016/j.apcata.2019.04.012>

Received 24 October 2018; Received in revised form 10 April 2019; Accepted 12 April 2019

Available online 17 April 2019

0926-860X/ © 2019 Elsevier B.V. All rights reserved.

hence activity of the Cu species [14–16]. An efficient strategy to overcome that is the incorporation of surface oxygen containing groups on carbon support, which can act as anchoring sites to improve the dispersion of Cu species and also promote the reduction of CuO to Cu₂O or Cu during the calcination process resulting in the improved catalytic activity [12,17]. However, the agglomeration and oxidation of Cu species occur easily during the reaction, resulting in the deactivation of catalysts [9,12,18]. Hence, obtaining the catalyst with higher catalytic activity and stability still remains the formidable challenge in state-of-the-art Cu based catalyst.

In recent years, N-doped carbon materials as the support have attracted much attention due to their unique properties [19–21]. The incorporation of surface nitrogen containing groups can enhance the hydrophilicity of carbon support, which allows the easy access of metal salt solutions to carbon surface [22]. Moreover, the surface nitrogen containing groups are regarded as more efficient and stable anchoring sites for metal species than the surface oxygen containing groups [23]. The surface oxygen containing groups, especially the carboxylic groups, could decompose during the calcination process resulting in the aggregation of metal species [24,25]. Whereas, the surface nitrogen containing groups play a crucial role in the stabilization of metal species [26–31]. Li et al. [29] concluded that the surface nitrogen containing groups inhibited the reduction of active center Au³⁺ to Au⁰ during the calcinations and acetylene hydrochlorination process, thus improved the catalytic activity and stability of Au/AC. Chen et al. [27] reported that the surface nitrogen containing groups on CNT improved the resistance of metallic Co against oxidation in ambient atmosphere. Bulusheva et al. [30] found that the surface nitrogen containing groups on CNF prevented the aggregation of Pt during the reaction process and thereby led to an excellent stability for hydrogen production from formic acid. Cabrele et al. [26] revealed that the surface nitrogen containing groups on CNT had successfully suppressed the leaching of Cu and thus improved the catalytic stability for A³-type coupling reactions.

This supports the fact that N-doping on carbon support could significantly overcome the limitations, viz., oxidation, aggregation and leaching of Cu species during the liquid phase oxidative carbonylation process. Generally, direct N-doping of the pristine carbon support results in low content of nitrogen containing groups due to the chemical inertness [28,32]. In the present work, we report a facile and efficient strategy to tune the contents of surface nitrogen containing groups on CNT by pre-oxidation and subsequent N-doping. The catalytic activity and stability of the obtained Cu/CNT catalysts are evaluated for liquid phase oxidative carbonylation of methanol to DMC. The influence of surface nitrogen containing groups on the dispersion and composition of Cu species as well as its stabilization during the oxidative carbonylation reaction are disclosed.

2. Experimental

2.1. Surface modification of the supports

2.1.1. Hydrothermal oxidation of the supports

The carbon nanotube (CNT, 0.5–2 μm long, ID = 5–10 nm, OD = 20–30 nm) was purchased from Chengdu Organic Chem. Co. Ltd. (Chinese Academy of Sciences). 1.5 g CNT was added into 75 mL nitric acid solution (0.5 mol/L) and the mixture was transferred to stainless steel autoclave for hydrothermal oxidative treatment. Firstly, the autoclave was sealed and pressurized to 0.8 Mpa with nitrogen. Subsequently, the temperature was gradually raised to 170 °C or 200 °C at a ramping rate of 2 °C/min and maintained for 4 h under stirring at a speed of 300 r/min. Then, the autoclave was cooled to RT and depressurized. The mixture was filtered and washed by distilled water until pH = 7. This was followed by drying in an oven at 100 °C for 10 h. The pristine CNT sample was denoted as CNT, while the oxidized CNT samples were denoted as OCNTX, where X represented the temperature

of hydrothermal oxidative treatment.

2.1.2. High temperature N-doping of the supports

Typically, 1 g CNT or OCNTX sample was ground with melamine keeping the mass ratio of melamine to CNT of 4. The mixture was annealed at 700 °C for 4 h in nitrogen atmosphere at a ramping rate of 2 °C/min. Finally, the N-doped CNT sample was washed by distilled water, filtered and dried at 100 °C for 10 h. The sample for N-doping of pristine CNT was denoted as NCNT, while the samples for N-doping of OCNTX were denoted as NCNTX, where X represents the temperature of hydrothermal oxidative treatment.

2.2. Preparation of the catalysts

The catalysts with 8 wt.% Cu loadings (nominal) were prepared using ultrasonic assisted impregnation. Firstly, 10 mL of Cu(NO₃)₂ aqueous solution was added dropwise to CNT supports. Subsequently, the mixture was ultrasonicated and stirred for 0.5 h followed by drying at 40 °C for 10 h and then calcined at 350 °C for 4 h in nitrogen atmosphere at a ramping rate of 2 °C/min. According to the different CNT supports, the obtained catalysts were denoted as Cu/CNT, Cu/NCNT, Cu/OCNTX and Cu/NCNTX.

2.3. Characterization of the supports and catalysts

The N₂ adsorption-desorption measurements were performed on a Beishide 3H-2000PS2 apparatus at –196 °C after outgassing the samples under vacuum at 250 °C for 4 h. The specific surface area of the samples were calculated by the Brunauer-Emmett-Teller (BET) method, and the pore size distribution was measured using the Barrett-Joyner-Halenda (BJH) model.

The X-ray photoelectron spectroscopy (XPS) data was collected on an ESCALab220i-XL electron spectrometer (VG, UK) using 300 W AlKα radiation. The samples were compressed into a pellet of 2 mm thickness and then mounted on a sample holder by utilizing double-sided adhesive tape for XPS analysis. The sample holder was then placed into a fast entry air load-lock chamber without exposure to air and evacuated under vacuum (< 10^{–6} Torr) over night. Finally, the sample holder was transferred to the analysis chamber for XPS study. The base pressure inside the analysis chamber was usually maintained at better than 10^{–10} Torr. The C1 s line (284.6 eV) was taken as a reference to correct for electrostatic charging.

The X-ray diffraction (XRD) measurements were performed on a Bruker D4 X-ray diffractometer with Ni filtered Cu Kα radiation (40 kV, 30 mA). The patterns were recorded in steps of 0.01° with the scanning rate at 4°/min from 5° to 85° under atmospheric pressure.

The actual Cu loading of the catalyst was determined with an inductively coupled plasma-optical emission spectrometer (ICP-OES 730, Agilent 7700). Before the measurements, ca. 100 mg prepared sample was dissolved in the mixture solutions with 0.5 mL hydrofluoric acid (40 wt %) and 2 mL concentrated nitric acid (65 wt %).

The transmission electron microscopy (TEM) photographs were taken with a JEOL JEM-2100 electron microscope, operating at 200 kV. The powder samples were ultrasonically dispersed in ethanol at room temperature for 30 min and transferred onto a carbon-coated copper grid by dipping. The mean particle diameters were determined by nano measurer software from TEM image analysis. Generally, at least 50 Cu nanoparticles per sample were selected to estimate their size distribution and the average particle size of Cu species.

The temperature-programmed reduction (TPR) experiments were carried out on Micromeritics Autochem 2920 equipment. Typically, 25 mg of catalyst was loaded into a U-shape quartz autoclave, and sample was degasified with argon (20 mL/min) at 200 °C for 2 h to remove physisorbed moisture. After cooling to room temperature, the gas was switched to 10% H₂ in argon flow (20 mL/min), and the temperature rose from 50 to 900 °C with a heating rate of 10 °C/min.

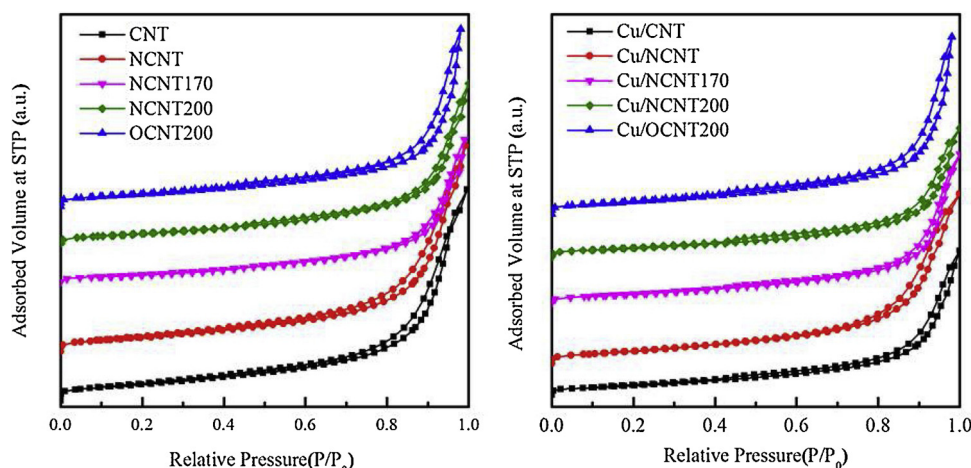


Fig. 1. N_2 adsorption-desorption isotherms of supports and the corresponding catalysts.

Effluent gas was passed through a cold trap to trap moisture in effluent gas before reaching the thermal conductivity detector (TCD).

The CH_3OH temperature-programmed desorption (CH_3OH -TPD) experiment was performed on a Micromeritics Autochem 2920 equipment. The sample was first degassed at $200^\circ C$ under helium flow (50 mL/min) for 1 h. After degassing, the temperature of the sample was maintained at $100^\circ C$. CH_3OH steam was then introduced to the sample cell (He as carrier gas) to allow the sample to absorb CH_3OH until saturated and then flushed with He to remove all physically adsorbed molecules. The temperature of the sample was raised from $100^\circ C$ to $300^\circ C$ at a rate of $10^\circ C/min$. The methanol released from the sample was continuously monitored by TCD.

The CO temperature-programmed desorption (CO-TPD) experiment was performed on a Micromeritics Autochem 2920 equipment. The sample was first degassed at $140^\circ C$ under helium flow (50 mL/min) for 1 h. Then, the sample was cooled to room temperature and saturated with CO. After removing the physically adsorbed CO by flushing with He, the sample was heated to $300^\circ C$ at a rate of $10^\circ C/min$ in He flow. The released CO from the sample was continuously monitored by TCD.

The total specific surface area and dispersion of Cu species were determined by N_2O titration in the same apparatus as for TPR. Firstly, the fresh catalysts were first reduced in the procedure described in the TPR experiment in a 10% H_2/Ar mixture until $450^\circ C$ and the reactor was purged with N_2 to $50^\circ C$. Then N_2O was used to oxidize surface copper atoms to Cu_2O (s). The specific surface area of Cu was performed by N_2O dissociative adsorption on the surface of copper with the pulse titration method based on the following equations: $2Cu$ (s) + $N_2O \rightarrow N_2 + Cu_2O$ (s). The evolution of N_2 was analyzed by thermal conductivity detector (TCD) to detect the consumption of N_2O (X). $S_{Cu} = 2XN_A(1+a)/1.4a \times 10^{19} (m^2/g_{Cu})$, where, N_A is Avogadro's constant, 1.4×10^{19} is the number of Cu atoms per square meter [33], a is the actual copper loading determined by ICP = m_{Cu}/m_{CNT} (%). Dispersion, $D = 2XM_{Cu}(1+a)/a$, where, M_{Cu} is the relative atomic mass of copper (63.46 g/mol).

2.4. Catalytic evaluation

The catalytic performance for liquid-phase oxidative carbonylation of methanol was evaluated in a 250 mL stainless-steel high-pressure autoclave under continuous mechanical stirring. Typically, 30 mL methanol and 0.3 g catalysts were placed into a stainless-steel autoclave. The autoclave was sealed and subsequently pressurized with CO up to 2 MPa and then by O_2 up to 3 MPa ($P_{CO}: P_{O_2}$ ratio of 2:1). The reaction temperature was gradually raised to $110^\circ C$ and maintained for 1.5 h. The liquid-phase samples and the catalysts were obtained by filtration after the autoclave was cooled to room temperature and depressurized.

The liquid-phase samples including dimethyl carbonate (DMC), methanol (MeOH), methyl formate (MF) and dimethoxymethane (DMM) were detected using an Agilent 6890 GC instrument equipped with FID detector. The response factor was defined as area/mole percent and that of DMC, MeOH, MF and DMM were 1.0257×10^3 , 7.1093×10^2 , 7.9139×10^2 and 1.7359×10^3 , respectively. To evaluate the stability of the catalysts, the catalysts were evaluated by repeating the experiment four times under the same conditions. The conversion of methanol (C_{MeOH}), the selectivity (S_{DMC}) and the space-time yield of DMC (STY_{DMC}) were defined as follows:

$$C_{MeOH} = \frac{\text{Amount of methanol converted (mol)}}{\text{Total amount of methanol (mol)}} \times 100\%$$

$$S_{DMC} = \frac{2 \times \text{Amount of DMC product (mol)}}{\text{Amount of methanol converted (mol)}} \times 100\%$$

$$STY_{DMC} = \frac{\text{Amount of DMC product (mg)}}{\text{Amount of catalyst (g)} \cdot t(\text{h})}$$

The turnover frequency of DMC (TOF) and the formation rate of DMC (R_{DMC}) were defined as follows:

$$TOF = \frac{\text{Amount of DMC product (mol)}}{n_{Cu} \times t}$$

$$\text{Rate} = \frac{\text{Amount of DMC product (mol)}}{S_{Cu} \times t}$$

3. Results and discussion

3.1. Textural properties of the supports and catalysts

The N_2 sorption isotherms of all the supports (Fig. 1) are classified as type IV with an obvious hysteresis loop at high relative pressures, indicating the presence of mesopores in the samples [34]. The similar N_2 sorption isotherms were observed for catalysts, suggesting the retention of CNT structure upon Cu loading. The detailed textural properties of supports and catalysts are summarized in the Table 1. The surface area and pore volume of NCNT, NCNT170, NCNT200, and OCNT200 are lower than that of CNT. This is mainly due to the introduction of surface oxygen or nitrogen containing groups upon chemical modification, which possibly blocks the entry of N_2 inside the pores [35,36]. The surface area, pore volume and average pore size of the supports decrease obviously after Cu loading, mainly owing to blocking of pores of the support upon the introduction of Cu species during the catalyst preparation [24,37]. Especially for CNT, the surface area and pore volume are $180 m^2/g$ and $0.85 cm^3/g$, while after Cu loading, the two parameters significantly decrease to $120 m^2/g$, and $0.58 cm^3/g$, respectively.

Table 1
Textural properties of the supports and catalysts.

Samples	BET Surface area (m ² g ⁻¹)	Pore volume (cm ³ g ⁻¹)	Average pore size (nm)
CNT	180	0.85	12.81
NCNT	171	0.83	12.60
NCNT170	136	0.75	15.19
NCNT200	134	0.65	13.08
OCNT200	147	0.71	13.02
Cu/CNT	120	0.58	12.31
Cu/NCNT	155	0.69	11.67
Cu/NCNT170	122	0.60	12.94
Cu/NCNT200	111	0.52	11.54
Cu/OCNT200	129	0.58	12.12

3.2. Surface chemistry of the supports

The surface chemistry of supports before and after Cu loading was characterized by XPS and the detailed results are listed in Table 2. The XPS survey spectra of supports are given in Fig. 2A. The peaks of C 1s and O 1s are detected in all supports, while the peak of N 1s is detected in N-doped supports including NCNT, NCNT170 and NCNT200. The peak intensity of O 1s increases with the elevated temperature of oxidative treatment, and the O atom percentage increases from 5.5% of CNT to 10.6% of OCNT200 (Table 2). This indicates that elevating the temperature of oxidative treatment could improve surface oxygen containing groups of support, which is consistent with the study reported by Silva et al. [38]. It is also seen from Fig. 2A that the peak intensity of N 1s increases with the O atom content of supports before N-doping, and the N atom percentage increases from 1.5% of NCNT to 5.2% of NCNT200 (Table 2). This evidently proves that the increase of surface oxygen containing groups of supports can effectively improve the nitrogen containing groups during the subsequent N-doping process. The reason may be the decomposition of surface oxygen containing groups could activate the adjacent C atom during the N-doping process, which is beneficial to the substitution C atom for N atom [39,40]. The corresponding elemental mapping images of Cu/NCNT200 (Fig. 5) indicates that N is homogeneously doped on the surface of NCNT200.

In order to demonstrate the anchoring effect of surface nitrogen containing groups for Cu species, the high-resolution N 1s spectra of supports (NCNT, NCNT170, NCNT200) and catalysts (Cu/NCNT, Cu/NCNT170, Cu/NCNT200) are presented in Fig. 2B and 2C. As presented in Fig. 2B, the binding energy centered at 398.2 eV, 399.7 eV and 404.2 eV corresponds to the pyridine N (N-6), pyrrole N (N-5) and pyridine oxide-N (N-O), respectively [41,42]. It is found that N-doping of CNT generates N-6 and N-5 groups, while N-doping of the oxidized CNT (OCNT170, OCNT200) introduces N-6, N-5 and N-O groups. The nitrogen containing groups are considered as anchoring sites for metal species, if the metal nanoparticles are selectively anchored on some kinds of nitrogen containing groups, the content of these groups would decrease after loading of metal species [43]. As seen from Fig. 2C, the

contents of N-6 and N-O groups decrease while that of N-5 groups increase after Cu loading. Especially for NCNT200, the contents of N-6 and N-O groups significantly decrease from 47.5% to 32.9% and from 31.0% to 18.1%, respectively, while the content of N-5 groups apparently increases from 21.5% to 49.0% (Table 2). This strongly support the inference that Cu species prefer to anchor on the N-6 and N-O groups rather than N-5.

3.3. XRD and TEM of the fresh catalysts

The XRD patterns of the fresh catalysts are shown in Fig. 3. The peaks at 26.1° and 43.1° correspond to the lattice planes of (002) and (100) of graphite structure in CNT (JCPDS. 41-1487). The peaks at 35.4°, 38.7°, 48.8° and 53.7° are attributed to the lattice planes of (002), (111), (202), and (020) in CuO (JCPDS. 44-0706), respectively, while the peaks at 61.5° and 65.7° are related to the lattice planes of (220) and (221) of Cu₂O (JCPDS. 05-0667). As shown in Fig. 3, the characteristic peaks of CuO are more intense than that of Cu₂O indicating the dominated Cu species are CuO in all the catalysts. Besides, it is clear that the intensity and width of characteristic peaks of CuO and Cu₂O tend to vary with the supports. It is found for all the catalysts that the peak width of CuO and Cu₂O broadens, while the peak intensity declines notably, after CNT treated by oxidation or N-doping when compared with Cu/CNT. This result suggests that oxidation or N-doping of CNT is favorable to the increased dispersion state of Cu species.

The dispersion state of Cu species was further characterized by TEM (Fig. 4) analysis. The particle size distribution and the average particle size are obtained by statistics at least 50 particles of each catalysts. As presented in Fig. 4(a), most of Cu species aggregate on the opening of CNT resulting in the formation of large Cu species particles except a small quantity of tiny particles. This is mainly due to the lack of anchoring sites for Cu species on the surface of CNT. However, for the CNT treated by oxidation or N-doping, the Cu species are uniformly dispersed on the surface with the particle size smaller than 5 nm (Fig. 4(b)-(e)). The XPS results show that oxidation or N-doping of CNT generates more surface oxygen or nitrogen containing groups, which enhances the hydrophilicity of CNT allowing the easy access of solutions during the impregnation process, meanwhile, provides the additional anchoring sites for metal species [22,44], and thus improves the dispersion of Cu species. The corresponding elemental mapping images of Cu/NCNT200 are presented in Fig. 5, which suggests that Cu species are homogeneously dispersed on the surface of NCNT200.

As presented in Fig. 4, the particle size distribution of Cu species becomes narrower and the average particle size gradually reduces with the increasing content of N. The average particle size of Cu species drastically decreases from 10.5 to 2.6 nm with the increasing content of N from 0 to 5.2%. Furthermore, the total contents of N and O for NCNT170 are 5.5%, while the content of O for OCNT200 is 10.5%. By comparison the particle size of Cu species for Cu/NCNT170 (3.8 nm) and that for Cu/OCNT200 (4.4 nm), it can be deduced that the surface nitrogen containing groups are more effective than oxygen containing groups for well dispersion of Cu species, which is also observed in our

Table 2
Surface compositions of carbon, oxygen and nitrogen for the samples obtained by XPS.

Samples	element composition (at.%)			percentage of different N containing groups (%)						
	C	O	N	before Cu loading			after Cu loading			
				N-6	N-5	N-O	N-6	N-5	N-O	
CNT	94.5	5.5	–	–	–	–	–	–	–	–
NCNT	90.4	8.1	1.5	38.8	61.2	–	20.7	79.3	–	–
OCNT170	92.2	7.8	–	–	–	–	–	–	–	–
NCNT170	94.5	2.4	3.1	33.4	46.7	19.9	29.3	58.3	12.4	–
OCNT200	89.4	10.6	–	–	–	–	–	–	–	–
NCNT200	89.1	5.7	5.2	47.5	21.5	31.0	32.9	49.0	18.1	–

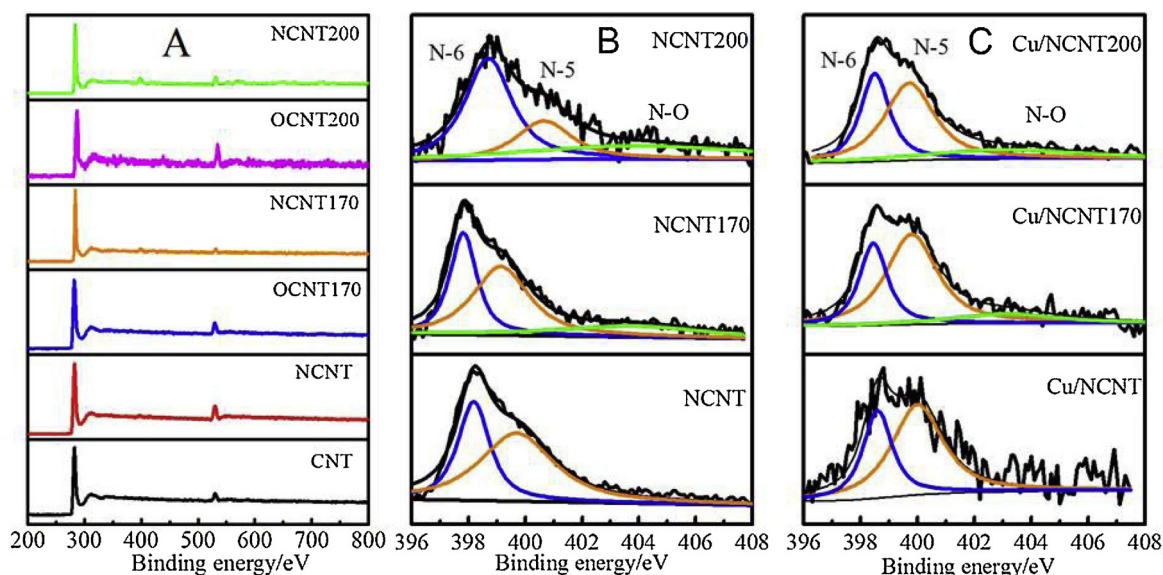


Fig. 2. XPS survey spectra of supports (A). High resolution N 1s XPS spectra of supports before (B) and after Cu loading (C).

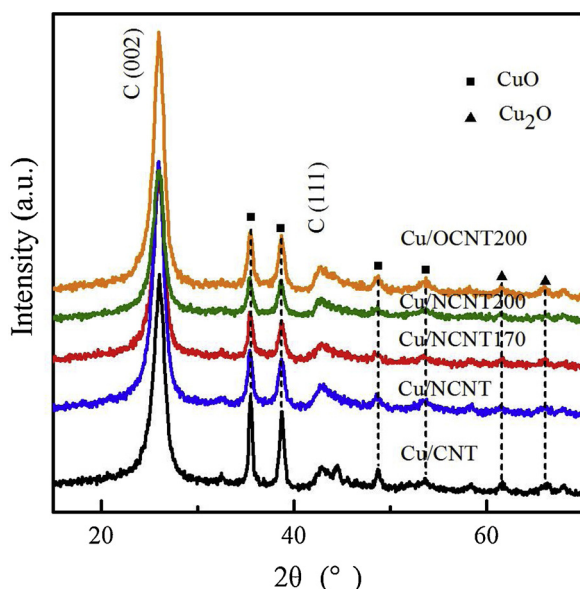


Fig. 3. XRD patterns of the fresh catalysts.

previous study [45]. The dispersion and surface area of Cu species were further quantitatively characterized by N_2O titration method as listed in Table 3. The dispersion and surface area of Cu species are largely dependent on the surface groups, and it apparently increases from 11.0% and $74.3 \text{ m}^2/\text{g}_{\text{Cu}}$ to 21.6% and $146.6 \text{ m}^2/\text{g}_{\text{Cu}}$, respectively, with the increasing content of N from 0 to 5.2%. This result is consistent with the XRD and TEM characterizations suggesting that the incorporation of surface nitrogen containing groups of CNT is an efficient strategy to improve the dispersion of Cu species.

3.4. XPS and TPR of the fresh catalysts

The surface composition of Cu species for catalysts was determined by XPS characterization. The Cu $2p_{3/2}$ XPS spectra and their gaussian fitting figures of catalysts are presented in Fig. 6. The Cu $2p_{3/2}$ spectra could be fitted into two peaks corresponding to Cu^{2+} and $(\text{Cu}^+ + \text{Cu}^0)$ for each catalysts. The binding energy in the range of 933.9–934.4 eV is assigned to Cu^{2+} , while that in the range of 932.1–932.9 eV is

attributed to $(\text{Cu}^+ + \text{Cu}^0)$ [46,47]. The percentage of the area of the peaks represents the relative amount of Cu^{2+} and $(\text{Cu}^+ + \text{Cu}^0)$ on the surface, and the result is presented in Table 4. The percentage of $(\text{Cu}^+ + \text{Cu}^0)$ increases after CNT treated by oxidation while declines after CNT treated by N-doping. Generally, the precursor of catalyst firstly decomposes to CuO during the calcination process, which is subsequently reduced to Cu_2O and Cu by carbon support [13,14]. It is found that the incorporation of oxygen containing groups on activated carbon promotes the auto-reduction of CuO to Cu_2O and Cu [12]. Besides, Yang et al. [44] found that the incorporation of oxygen containing groups on ordered mesoporous carbon promoted the auto-reduction of CoO to Co. Our results are in good agreement with these reports. On the other hand, it is noteworthy that the percentage of $(\text{Cu}^+ + \text{Cu}^0)$ gradually decreases from 38.0 to 29.2% with the increasing content of N from 0 to 5.2%. Similarly, Yang et al. [43] reported that the incorporation of nitrogen containing groups on ordered mesoporous carbons had improved the temperature of auto-reduction for CoO, which was detrimental for the auto-reduction of CoO to Co. This result implies that the incorporation of nitrogen containing groups enhances the interaction between CuO and CNT, which suppresses the auto-reduction of CuO to Cu_2O and Cu during the calcination process.

The H_2 -TPR was carried out to elucidate the bulk compositions and the state of Cu species of the catalysts. As shown in Fig. 7, all the catalysts exhibit one obvious peak with temperature lower than 250°C , which is assigned to the reduction of CuO [48]. Besides, this very weak peak at the temperature higher than 500°C is attributed to the gasification of the carbon support [49]. It is apparent that the dominated Cu species are CuO in these catalysts, which is consistent with the XRD and XPS characterizations. It should be noted that Cu_2O was detected by XRD and XPS characterizations, however, no obvious reduction peak for Cu_2O is observed in the H_2 -TPR profiles of these catalysts. This suggests the presence of low concentration of Cu_2O on the surface of these catalysts. Furthermore, after the treatment of CNT by oxidation or N-doping, the reduction temperature of CuO becomes lower following the sequence: Cu/CNT (214.4°C) > $\text{Cu}/\text{OCNT200}$ (190.6°C) \approx Cu/NCNT (189.6°C) > $\text{Cu}/\text{NCNT170}$ (180.6°C) > $\text{Cu}/\text{NCNT200}$ (177.4°C). Generally, the reduction temperature of metal species is closely related to its dispersion state over support, and the metal species with higher dispersion are more easily reduced in H_2 atmosphere [44,48,50,51]. This is due to the fact that the incorporated surface oxygen or nitrogen containing groups enhances the interaction between

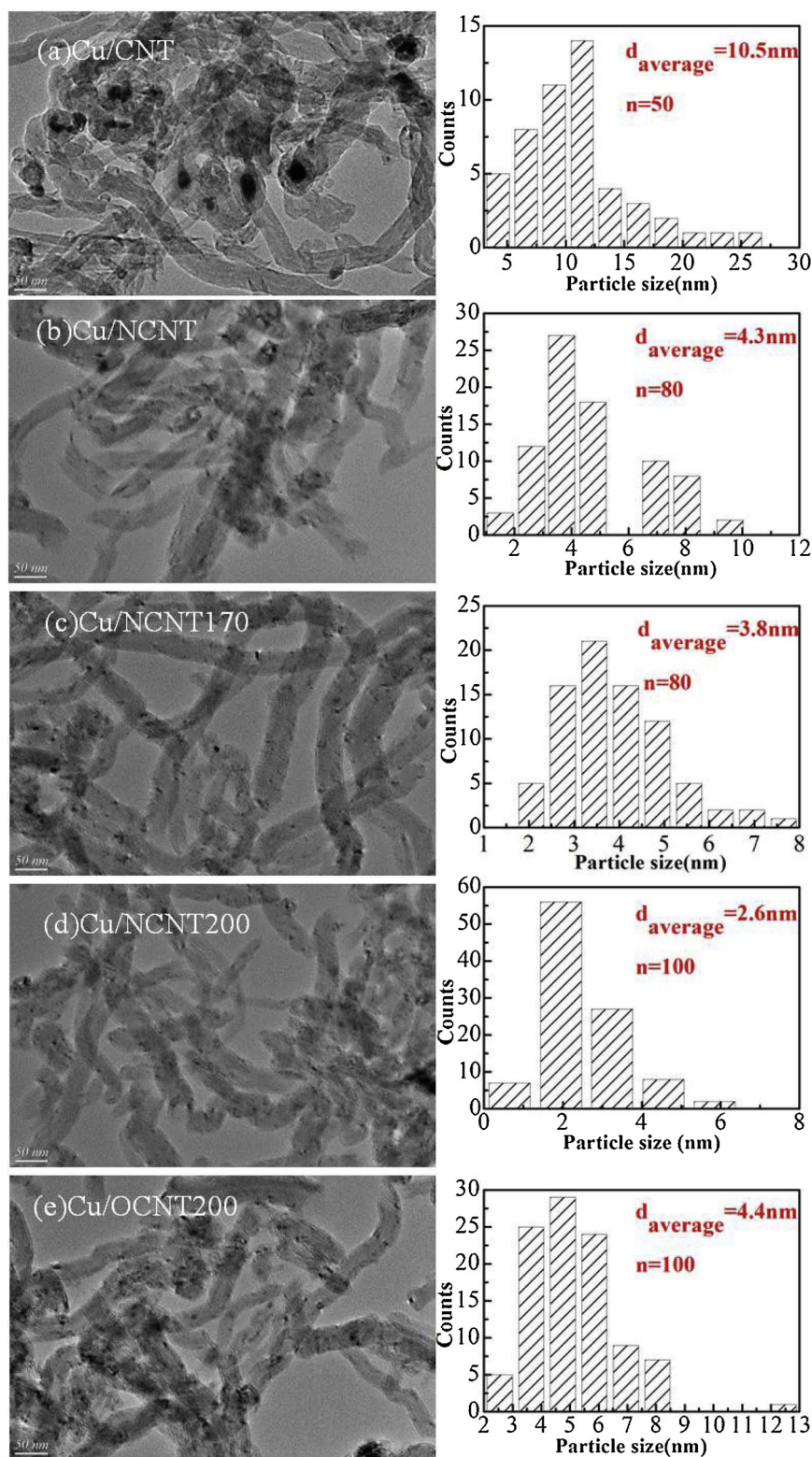


Fig. 4. Representative TEM images and particle size distribution histograms of the fresh catalysts (a) Cu/CNT, (b) Cu/NCNT, (c) Cu/NCNT170, (d) Cu/NCNT200, (e) Cu/OCNT200.

the support and the precursor resulting in the formation of smaller CuO particles, which is in good agreement with the TEM and N_2O titration analyses of the catalysts.

3.5. Catalytic activity and stability

The catalytic performance of catalysts for liquid phase oxidative carbonylation of methanol is given in Table 5. It is well known that the dispersion of Cu species plays a crucial role on the catalytic performance of catalysts for oxidative carbonylation of methanol

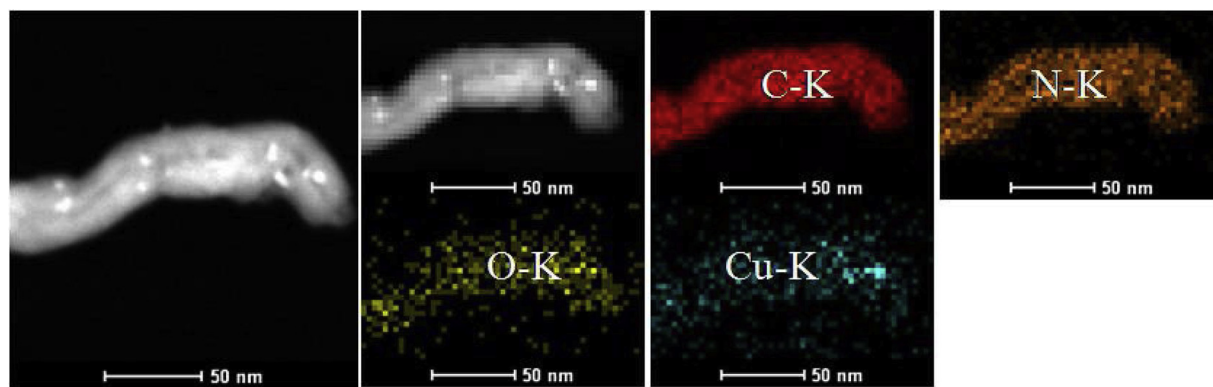


Fig. 5. Representative STEM images of Cu/NCNT200 and corresponding elemental mapping images of C, O, N and Cu elements.

Table 3
Surface areas and dispersion of Cu species determined by N_2O titration.

Samples	Cu dispersion(%)	S_{Cu} (m^2/g_{Cu})
Cu/CNT	11.0	74.3
Cu/NCNT	13.7	92.8
Cu/NCNT170	16.1	108.8
Cu/NCNT200	21.6	146.6
Cu/OCNT200	14.5	98.2

[12,15,18,52]. As seen from Table 5, the Cu/CNT catalyst shows poor catalytic performance. The conversion of methanol (C_{MEOH}), selectivity of DMC (S_{DMC}) and space-time yield of DMC (STY_{DMC}) are 0.25%, 80.6% and $150.5 \text{ mg g}^{-1} \text{ h}^{-1}$, respectively. However, dramatic improvement of catalytic performance is observed in terms of C_{MEOH} , S_{DMC} and STY_{DMC} , after the modification of CNT by oxidation or N-doping. This is mainly due to the increased dispersion of Cu species upon modifications as evidenced from TEM and N_2O titration. For the Cu/OCNT200 catalyst, the C_{MEOH} and STY_{DMC} reach 1.3% and $873.0 \text{ mg g}^{-1} \text{ h}^{-1}$, which are five times more than that of Cu/CNT catalyst. For the N-doped catalysts, the C_{MEOH} and STY_{DMC} for Cu/NCNT, Cu/NCNT170 and Cu/NCNT200 are four times, six times and ten times more than that of Cu/CNT catalyst, respectively. Among these catalysts, Cu/NCNT200 shows the optimal catalytic performance, and the C_{MEOH} and STY_{DMC} achieve 2.4% and $1789.6 \text{ mg g}^{-1} \text{ h}^{-1}$, which are nearly twice as that of Cu/OCNT200.

The catalytic performances of other Cu-based catalysts reported previously are also presented in Table 5 for comparison. It is worth noticing that Cu species are mainly present in the form of CuO in this study, while the dominated Cu species were Cu_2O or Cu in the recently reported studies [10,11,52–54]. In general, the catalytic performance of Cu_2O or Cu is better than that of CuO [14,16]. Even though, it is apparent that Cu/NCNT200 shows better catalytic performance than Cu/MSC [53], Cu/NG [54] and Cu@NHCSs [52] in terms of STY_{DMC} and TOF. The result may be due to the fact that the particle size of Cu species in Cu/NCNT200 (2.6 nm) is much smaller than that of Cu/MSC (3.8 nm), Cu/NG (7.5 nm) and Cu@NHCSs (7.4 nm) [52–54], and the activity of Cu species with small particle size is better than that with larger ones.

In addition to the particle size effect, the promoting effect of surface nitrogen containing groups should be taken into consideration too. It has been proved that incorporation of surface nitrogen containing groups enhanced the charge transfer of Cu species to graphene resulting in the decrease of gas adsorption free energy [54]. Recently, the reaction mechanism of Cu, Cu_2O and CuO for oxidative carbonylation of methanol to DMC has been proposed successively [55–57]. The reaction mechanisms of Cu and Cu_2O are the same and proceed according to the following steps. Firstly, CH_3OH is adsorbed and dissociated with the formation of CH_3O species. Secondly, adsorption and insertion of

carbon monoxide into the CH_3O species lead to the formation of CH_3OCO species as an intermediate, which is the rate-limiting step of DMC formation. At the end, the CH_3OCO species react with CH_3O species to form DMC [55,57]. However, the reaction mechanism of CuO is different from that of Cu and Cu_2O . Firstly, CH_3OH is adsorbed and dissociated with the formation of CH_3O species. Then, two CH_3O species react and form $(CH_3O)_2$ species as an intermediate. At last, adsorption and insertion of carbon monoxide into the $(CH_3O)_2$ species lead to the formation of DMC, which is the rate-limiting step of DMC formation [56]. From the viewpoint of reaction mechanism, the adsorption properties of CO and CH_3OH play a vital role on the catalytic performance of the catalysts. Considering that, CO-TPD and CH_3OH -TPD characterizations were carried out and the results are presented in Fig. 8. Obviously, the adsorption capacities of CO and CH_3OH are greatly enhanced after the modification of CNT by oxidation or N-doping and attain maximum for Cu/NCNT200.

The catalytic performance of Cu species anchored on different nitrogen containing groups of graphene is compared by DFT, and the pyridine N groups are considered as the most efficient anchoring site for Cu species in oxidative carbonylation of methanol [58]. The N 1s XPS results of supports and catalysts confirm that Cu species prefer to anchor on the pyridine N groups of CNT. Hence, it is reasonable to deduce that the superior catalytic performance of Cu/NCNT200 is attributed to the small particle size of Cu species and the promoting effect of pyridine N groups.

To further explore the influence of surface nitrogen containing groups, the stability of consecutive four runs was also evaluated and the results are presented in Table 5. After each cycle, the used catalysts were collected by filtration and then washed with methanol. After dried in vacuum overnight, the catalytic performance of catalysts was re-evaluated under the identical conditions. As seen from Table 5, the C_{MEOH} , STY_{DMC} and TOF of all catalysts drop to some extent with the increased number of catalytic cycles. After consecutive four recycles, the declined degrees in terms of STY_{DMC} for Cu/CNT, Cu/NCNT, Cu/NCNT170, Cu/NCNT200 and Cu/OCNT200 are 42.3%, 33.4%, 25.2%, 12.9% and 39.8%, respectively, with respect to their initial values (Fig. 9). While, the declined degrees in terms of TOF for Cu/CNT, Cu/NCNT, Cu/NCNT170, Cu/NCNT200 and Cu/OCNT200 are 29.4%, 26.3%, 19.2%, 9.7% and 33.7%, respectively. This further supports the fact that the stability of the catalyst is increased to a great extent upon modification of CNT with the surface nitrogen containing groups.

3.6. Characterization of the used catalysts

Generally, the agglomeration of Cu species is responsible for the decline in the catalytic performance of Cu-based catalysts [59]. Since the reaction of oxidative carbonylation of methanol was performed under the CO and O_2 environment, the chemical state of Cu species may change during the reaction process. As the evaluation of catalytic

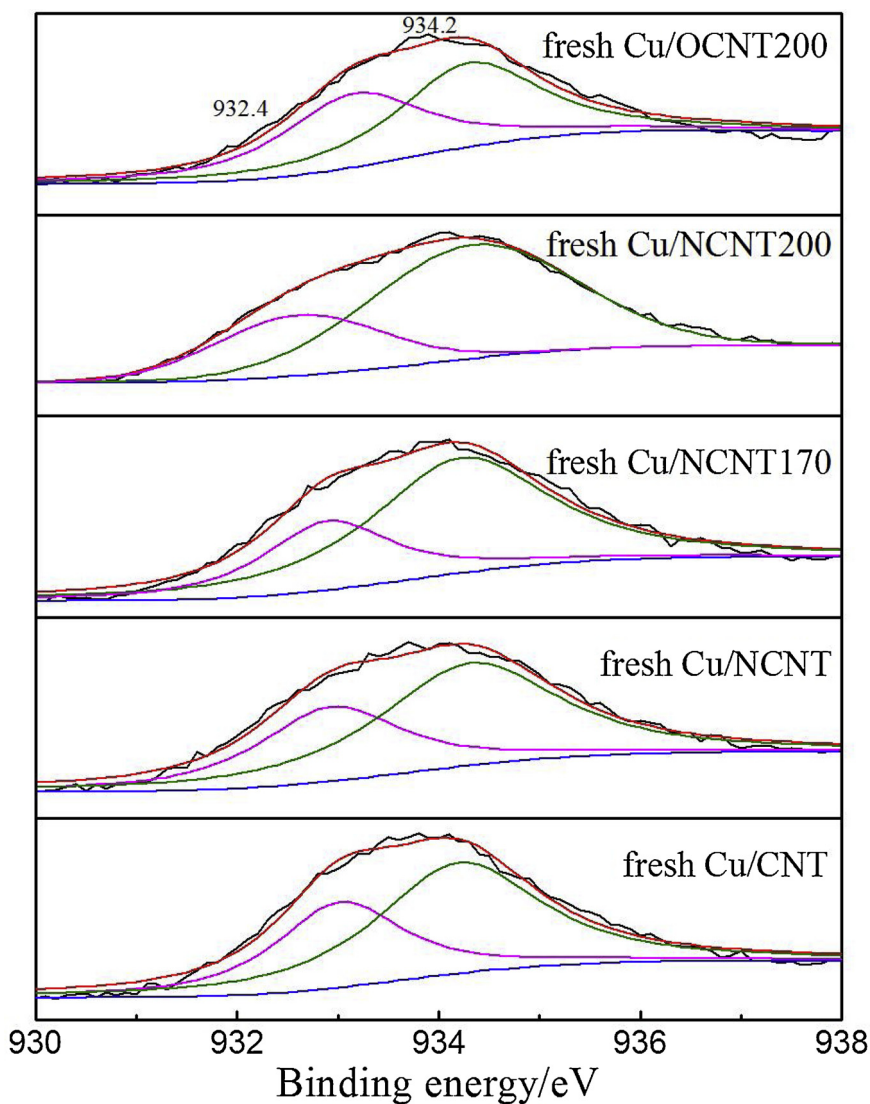


Fig. 6. $\text{Cu}2p_{3/2}$ XPS spectra of the fresh catalysts.

Table 4
Surface Cu compositions of the catalysts based on $\text{Cu}2p_{3/2}$ XPS deconvolution.

Samples	BE of $\text{Cu}2p_{3/2}/\text{eV}$	Area percentage of $\text{Cu}2p_{3/2}/\%$				$R(\text{Cu}^+ + \text{Cu}^0)$
		$\text{Cu}^+ + \text{Cu}^0$	Cu^{2+}	$\text{Cu}^+ + \text{Cu}^0$	$R(\text{Cu}^+ + \text{Cu}^0)$	
Fresh Cu/CNT	934.2	932.9	62.0	38.0	–	
Fresh Cu/NCNT	934.3	932.9	62.9	37.1	–	
Fresh Cu/NCNT170	934.2	932.9	69.5	30.5	–	
Fresh Cu/NCNT200	934.2	932.6	70.8	29.2	–	
Fresh Cu/OCNT200	934.2	932.9	53.3	46.7	–	
Used Cu/CNT	934.2	932.5	75.6	24.4	35.8	
Used Cu/NCNT	934.4	932.8	68.0	32.0	13.7	
Used Cu/NCNT170	934.3	932.5	72.6	27.4	10.2	
Used/NCNT200	933.9	932.1	71.3	28.7	1.7	
Used Cu/OCNT200	934.2	932.6	69.3	30.7	34.2	

$R(\text{Cu}^+ + \text{Cu}^0)$ represented the declined degree of $(\text{Cu}^+ + \text{Cu}^0)$ after reaction.

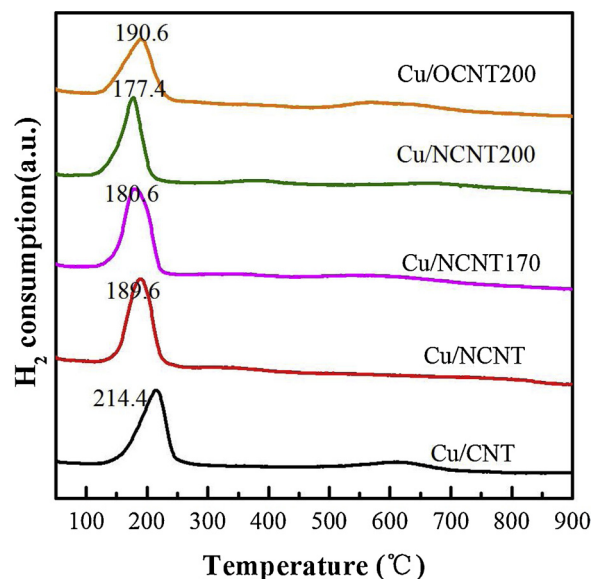


Fig. 7. H_2 -TPR profiles of the fresh catalysts.

Table 5
Catalytic performance for liquid-phase oxidative carbonylation of methanol.

Catalysts	C _{MeOH} (%)	S _{DMC} (%)	S _{DMM} (%)	S _{MF} (%)	STY _{DMC} (mg g ⁻¹ h ⁻¹)	Rate (mol m ⁻² s ⁻¹)	TOF (h ⁻¹)
Cu/CNT ^{1st}	0.25	80.6	2.2	17.2	150.5	1.0 × 10 ⁻⁷	1.7
Cu/CNT ^{2nd}	0.23	72.1	4.1	23.8	125.0	–	–
Cu/CNT ^{3rd}	0.20	70.6	10.9	18.5	101.5	–	–
Cu/CNT ^{4th}	0.17	67.0	2.1	30.9	86.9	–	1.2
Cu/NCNT ^{1st}	1.01	95.1	0.6	4.3	711.3	3.6 × 10 ⁻⁷	7.6
Cu/NCNT ^{2nd}	0.87	93.7	0.7	5.6	607.7	–	–
Cu/NCNT ^{3rd}	0.78	93.7	0.5	5.8	550.3	–	–
Cu/NCNT ^{4th}	0.67	94.5	0.4	5.1	473.5	–	5.6
Cu/NCNT170 ^{1st}	1.71	96.9	0.4	2.7	1241.3	5.0 × 10 ⁻⁷	12.5
Cu/NCNT170 ^{2nd}	1.55	95.9	0.4	3.7	1115.3	–	–
Cu/NCNT170 ^{3rd}	1.35	96.8	0.3	2.9	982.6	–	–
Cu/NCNT170 ^{4th}	1.28	96.5	0.3	3.2	928.5	–	10.1
Cu/NCNT200 ^{1st}	2.44	97.8	0.3	1.9	1789.6	5.2 × 10 ⁻⁷	17.6
Cu/NCNT200 ^{2nd}	2.37	96.8	0.5	2.7	1724.1	–	–
Cu/NCNT200 ^{3rd}	2.26	97.4	0.3	2.3	1649.7	–	–
Cu/NCNT200 ^{4th}	2.13	97.4	0.4	2.2	1557.9	–	15.9
Cu/OCNT200 ^{1st}	1.30	89.8	1.5	8.7	873.0	3.9 × 10 ⁻⁷	8.9
Cu/OCNT200 ^{2nd}	1.06	95.5	0.5	4.0	758.5	–	–
Cu/OCNT200 ^{3rd}	0.86	92.7	0.6	6.7	594.8	–	–
Cu/OCNT200 ^{4th}	0.75	93.8	0.5	5.7	525.0	–	5.9
Cu/MS [53]	1.5	89.2	–	–	495.1	–	–
Cu/NG [54]	3.1	97.6	0.4	2.0	1665.0	–	16.9
Cu@NHCSs [52]	2.1	96.6	1.3	2.1	1528.0	–	11.0

performance of catalysts was carried out under stirring condition, the leaching of Cu may occur during the reaction process. Hence, the dispersion state, chemical state and content of Cu species of the used catalysts after consecutive four recycles were further characterized by TEM, XPS and ICP.

Fig. 10 shows the representative TEM images of the used catalysts. Significant agglomeration of Cu species is observed for the used Cu/CNT (Fig. 10a). It is apparent that the degree of agglomeration is decreased upon incorporation of surface oxygen or nitrogen containing groups. As presented in Fig. 10b and Fig. 10e, the slight agglomeration is observed for the used Cu/OCNT200 and Cu/NCNT. It should be noted that no obvious agglomeration is found in the used Cu/NCNT170 and Cu/NCNT200 (Fig. 10c and Fig. 10d) and the average particle size of Cu species slightly increases from 3.8 to 5.5 nm and 2.6 to 2.8 nm, respectively. This result suggests that the incorporation of surface nitrogen containing groups effectively suppresses the agglomeration and growing of Cu species, and this effect becomes more remarkable for those with higher content of N.

The actual Cu loading of catalysts before and after reaction were analyzed by ICP-OES as presented in Fig. 11. It is observed that the actual Cu loading of fresh catalysts increases with the increasing

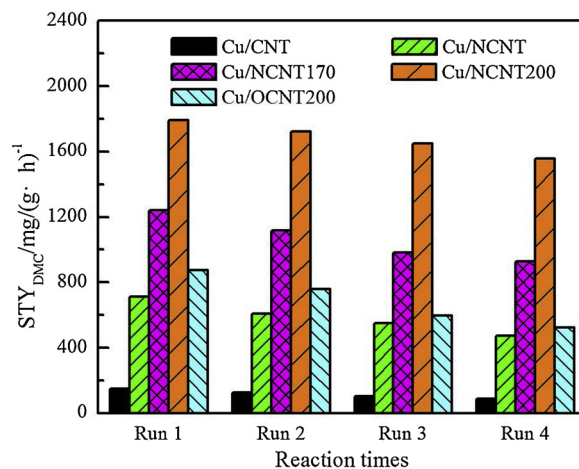


Fig. 9. Stability of the catalysts.

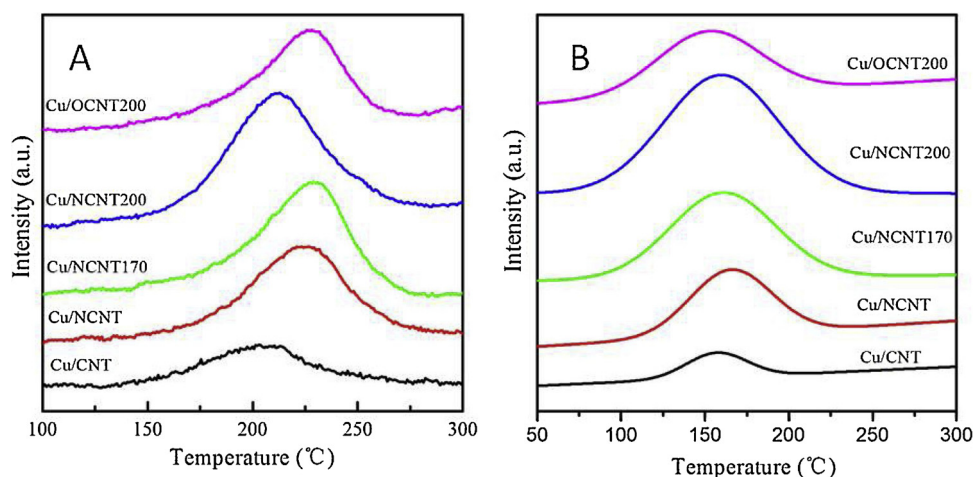


Fig. 8. CH₃OH-TPD (A) and CO-TPD (B) profiles of the catalysts.

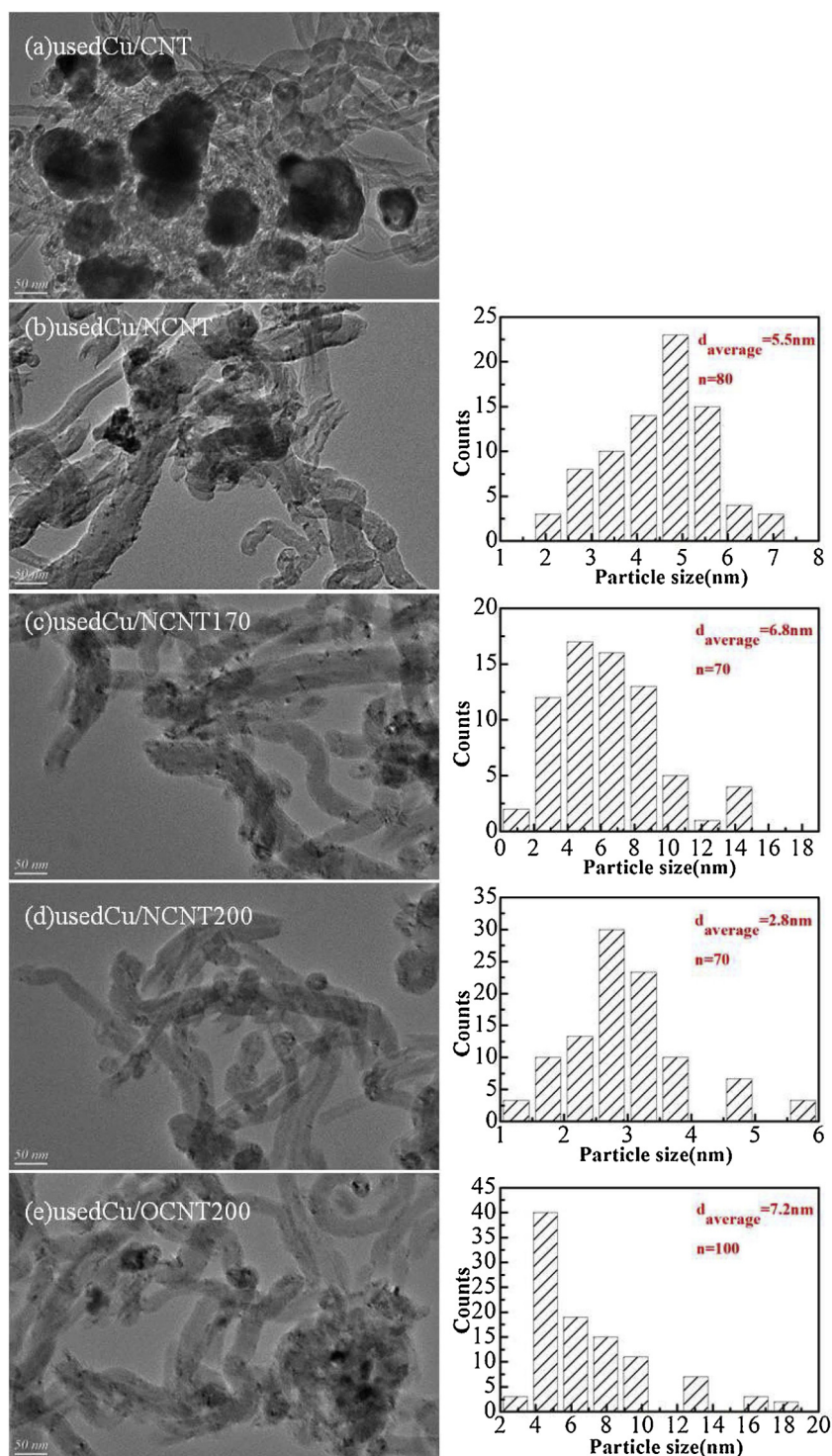


Fig. 10. Representative TEM images and particle size distribution histograms of the used catalysts (a) used Cu/CNT, (b) used Cu/NCNT, (c) used Cu/NCNT170, (d) used Cu/NCNT200, (e) used Cu/OCNT200.

content of N, and that attains the highest (7.8%) when the content of N is 5.2%, which is very close to the nominal Cu loading (8.0%). This is a result of the increased anchoring sites originating from surface nitrogen containing groups. The content of Cu drops to some extent for all catalysts indicating the leaching of Cu occurred during the reaction process. The leaching levels of Cu for Cu/CNT, Cu/NCNT, Cu/NCNT170, Cu/NCNT200 and Cu/OCNT200 are 16.4%, 9.9%, 7.1%, 3.8% and 7.0%, respectively. This suggests that the incorporation of surface nitrogen containing groups effectively suppresses the leaching of Cu

species due to the enhanced interaction between CNT and Cu species, especially for those with higher content of N.

In general, the catalytic reaction proceeds on the surface of catalysts, and hence the analysis of change for surface Cu species is essential to better understand the decline of the catalytic performance. The Cu $2p_{3/2}$ XPS spectra and their gaussian fitting figures of the used catalysts are presented in Fig. 12. It is found that the content of $(Cu^{+} + Cu^{0})$ decreases while that of Cu^{2+} increases for all the catalysts after reaction (Table 4). This result indicates that the Cu species tend to be oxidized

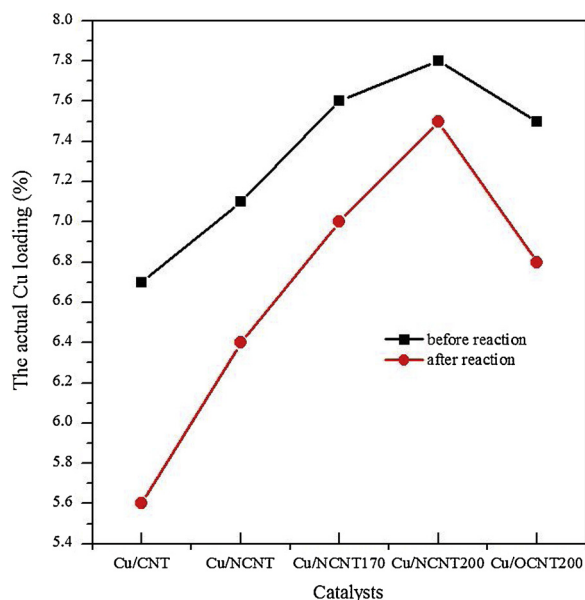


Fig. 11. The actual Cu loading of catalysts before and after reaction.

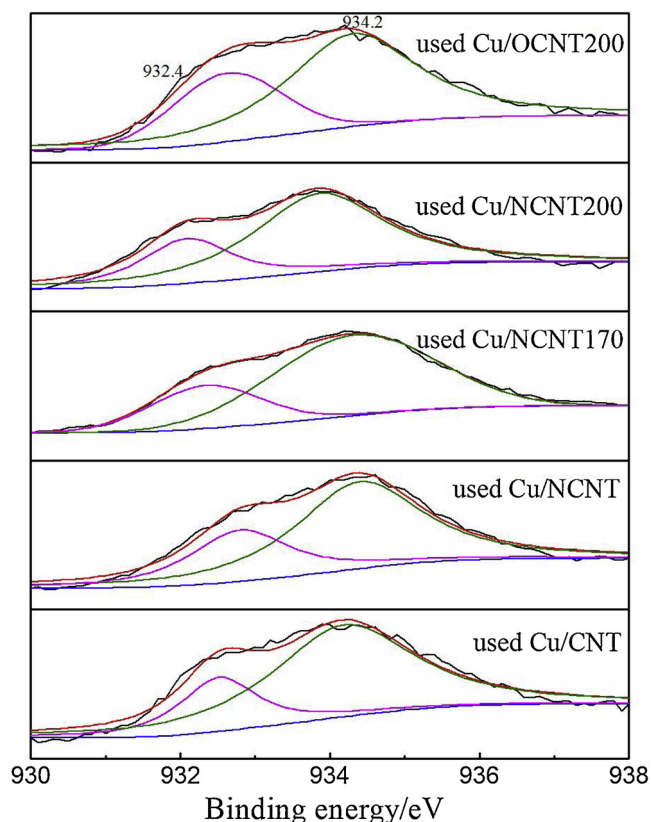


Fig. 12. $\text{Cu}2p_{3/2}$ XPS spectra of the used catalysts.

rather than reduced during the reaction. Moreover, the degree of oxidation varies with the change of surface groups. The decreasing extents of ($\text{Cu}^+ + \text{Cu}^0$) for Cu/CNT, Cu/NCNT, Cu/NCNT170, Cu/NCNT200 and Cu/OCNT200 are 35.8%, 13.7%, 10.2%, 1.7% and 34.2%, respectively. This result proves that the increase of surface nitrogen containing groups effectively suppresses the oxidation of Cu species during the reaction process.

Chen et al. [27] found that the incorporation of surface nitrogen containing groups on CNT improved the resistance of metallic Co

against oxidation in ambient atmosphere. Recently, Wang et al. [60] revealed that Ru nanoparticles supported on N-doped hierarchically porous carbon were stable even aging in air for one year. Our results are consistent with these reports. The possible reason is that the enriched electron density of nitrogen containing groups has inhibited electron transfer from Cu_2O to O_2 and thus suppressed the oxidation of Cu species. It is noteworthy that the dominated Cu species are CuO in this study, however, the activity of surface Cu_2O of catalysts should not be ignored. Therefore, the oxidation of Cu species is also considered as one of the factors leading to the decline in catalytic performance. Based on the factors discussed above, it can be deduced that the superior stability of Cu/NCNT200 is due to the enhanced anti-agglomeration, anti-oxidation and anti-leaching properties of Cu species.

4. Conclusions

The CNTs containing different levels of N were successfully prepared by pre-oxidation and subsequent N-doping at high temperature. The incorporated surface oxygen containing groups by pre-oxidation effectively improve the content of N on CNT during the subsequent N-doping process. The nitrogen containing groups, especially the pyridine N groups, serving as the preferred anchoring sites, significantly promote the dispersion of Cu species. The superior catalytic performance of Cu/NCNT200 is attributed to the small particle size of Cu species and the promoting effect of pyridine N groups. Furthermore, the presence of N containing groups strengthen the interaction between CNT and Cu species, which overcome the limitations, viz., agglomeration, oxidation and leaching of Cu species during the reaction process and thus improves the stability of catalysts. The catalyst, Cu/NCNT200 shows the optimal stability due to the highest level of N doping.

Acknowledgements

The authors are grateful for the financial support from the National Natural Science Foundation of China (U1510203) and Natural Science Foundation of Shanxi Province (201701D221043) and Major Projects of Shanxi Province (MC2015-04).

References

- [1] S. Huang, B. Yan, S. Wang, X. Ma, Chem. Soc. Rev. 44 (2015) 3079–3116.
- [2] R. Saada, O. AboElazayem, S. Kellici, T. Heil, D. Morgan, G.I. Lampronti, B. Saha, Appl. Catal. B 226 (2018) 451–462.
- [3] P. Yang, Y. Cao, W.-L. Dai, J.-F. Deng, K.-N. Fan, Appl. Catal. A Gen. 243 (2003) 323–331.
- [4] T.T.H. Dang, M. Bartoszek, M. Schneider, D.-L. Hoang, U. Bentrup, A. Martin, Appl. Catal. B 121–122 (2012) 115–122.
- [5] M. Richter, M.J.G. Fait, R. Eckelt, E. Schreiber, M. Schneider, M.M. Pohl, R. Fricke, Appl. Catal. B 73 (2007) 269–281.
- [6] M.S. Han, B.G. Lee, I. Suh, H.S. Kim, B.S. Ahn, S.I. Hong, J. Mol. Catal. A Chem. 170 (2001) 225–234.
- [7] B. Yan, S.Y. Huang, Q.S. Meng, Y.L. Shen, S.P. Wang, X.B. Ma, *AIChE J.* 59 (2013) 3797–3805.
- [8] X. Ding, X. Dong, D. Kuang, S. Wang, X. Zhao, Y. Wang, Chem. Eng. J. 240 (2014) 221–227.
- [9] G. Zhang, J. Yan, J. Wang, D. Jia, H. Zheng, Z. Li, Appl. Surf. Sci. 455 (2018) 696–704.
- [10] K. Shi, S.-Y. Huang, Z.-Y. Zhang, S.-P. Wang, X.-B. Ma, Chin. Chem. Lett. 28 (2017) 70–74.
- [11] B. Yan, S.Y. Huang, S.P. Wang, X.B. Ma, Chemcatchem 6 (2014) 2671–2679.
- [12] G. Zhang, Z. Li, H. Zheng, T. Fu, Y. Ju, Y. Wang, Appl. Catal. B 179 (2015) 95–105.
- [13] J. Ren, M. Ren, D. Wang, J. Lin, Z. Li, J. Therm. Anal. Calorim. 120 (2015) 1929–1939.
- [14] R. Wang, Z. Li, H. Zheng, K. Xie, Chin. J. Catal. 31 (2010) 851–856.
- [15] M. Ren, J. Ren, P. Hao, J. Yang, D. Wang, Y. Pei, J.Y. Lin, Z. Li, Chemcatchem 8 (2016) 861–871.
- [16] Z. Li, C. Wen, R. Wang, H. Zheng, K. Xie, Chem. J. Chin. U. 30 (2009) 2024–2031.
- [17] J. Wang, R. Shi, P. Hao, W. Sun, S. Liu, Z. Li, J. Ren, J. Mater. Sci. 53 (2018) 1833–1850.
- [18] T. Fu, X. Wang, H. Zheng, Z. Li, Carbon 115 (2017) 363–374.
- [19] R. Nie, M. Miao, W. Du, J. Shi, Y. Liu, Z. Hou, Appl. Catal. B 180 (2016) 607–613.
- [20] A.B. Ayusheev, O.P. Taran, I.A. Seryak, O.Y. Podyacheva, C. Descorme, M. Besson, L.S. Kibis, A.I. Boronin, A.I. Romanenko, Z.R. Ismagilov, V. Parmon, Appl. Catal. B

- 146 (2014) 177–185.
- [21] Y.L. Cao, S.J. Mao, M.M. Li, Y.Q. Chen, Y. Wang, *ACS Catal.* 7 (2017) 8090–8112.
- [22] G. Bae, D.H. Youn, S. Han, J.S. Lee, *Carbon* 51 (2013) 274–281.
- [23] L.M. Chew, W. Xia, H. Düdder, P. Weide, H. Ruland, M. Muhler, *Catal. Today* 270 (2016) 85–92.
- [24] G. Zhang, Z. Li, H. Zheng, Z. Hao, X. Wang, J. Wang, *Appl. Surf. Sci.* 390 (2016) 68–77.
- [25] S.A. Chernyak, E.V. Suslova, A.S. Ivanov, A.V. Egorov, K.I. Maslakov, S.V. Savilov, V.V. Lunin, *Appl. Catal. A Gen.* 523 (2016) 221–229.
- [26] V.G. Ramu, A. Bordoloi, T.C. Nagaiah, W. Schuhmann, M. Muhler, C. Cabrele, *Appl. Catal. A Gen.* 431–432 (2012) 88–94.
- [27] P. Chen, F. Yang, A. Kostka, W. Xia, *ACS Catal.* 4 (2014) 1478–1486.
- [28] W. Zhao, W. Li, J. Zhang, *Catal. Sci. Technol.* 6 (2016) 1402–1409.
- [29] J. Zhao, J. Xu, J. Xu, T. Zhang, X. Di, J. Ni, X. Li, *Chem. Eng. J.* 262 (2015) 1152–1160.
- [30] D.A. Bulushev, M. Zacharska, A.S. Lisitsyn, O.Y. Podyacheva, F.S. Hage, Q.M. Ramasse, U. Bangert, L.G. Bulusheva, *ACS Catal.* 6 (2016) 3442–3451.
- [31] J. Liang, X. Zhang, L. Jing, H. Yang, *Chin. J. Catal.* 38 (2017) 1252–1260.
- [32] Y. Sun, L. Chen, Y. Bao, G. Wang, Y. Zhang, M. Fu, J. Wu, D. Ye, *Catal. Today* 307 (2018) 212–223.
- [33] S. Xia, R. Nie, X. Lu, L. Wang, P. Chen, Z. Hou, *J. Catal.* 296 (2012) 1–11.
- [34] T. Fu, R. Liu, J. Lv, Z. Li, *Fuel. Process. Technol.* 122 (2014) 49–57.
- [35] E.G. Rodrigues, M.F.R. Pereira, X. Chen, J.J. Delgado, J.J.M. Órfão, *J. Catal.* 281 (2011) 119–127.
- [36] C.Y. Yin, M.K. Aroua, W.M.A.W. Daud, *Sep. Purif. Technol.* 52 (2007) 403–415.
- [37] V. Priyanka, V.C. Subbaramaiah, I.D. Srivastava, *Mall, Sep. Purif. Technol.* 125 (2014) 284–290.
- [38] R.R.N. Marques, B.F. Machado, J.L. Faria, A.M.T. Silva, *Carbon* 48 (2010) 1515–1523.
- [39] M.S. Shafeeyan, W.M.A.W. Daud, A. Houshmand, A. Arami-Niya, *Appl. Surf. Sci.* 257 (2011) 3936–3942.
- [40] M.H. Kasnejad, A. Esfandiari, T. Kaghazchi, N. Asasian, *J. Taiwan. Inst. Chem. Eng.* 43 (2012) 736–740.
- [41] T. Horikawa, N. Sakao, T. Sekida, Ji. Hayashi, D.D. Do, M. Katoh, *Carbon* 50 (2012) 1833–1842.
- [42] J. Zhang, Y. Song, M. Kopeć, J. Lee, Z. Wang, S. Liu, J. Yan, R. Yuan, T. Kowalewski, M.R. Bockstaller, K. Matyjaszewski, *J. Am. Chem. Soc.* 139 (2017) 12931–12934.
- [43] Y. Yang, L. Jia, B. Hou, D. Li, J. Wang, Y. Sun, *Chemcatchem* 6 (2014) 319–327.
- [44] Y. Yang, L. Jia, B. Hou, D. Li, J. Wang, Y. Sun, *Catal. Sci. Technol.* 4 (2014) 717–728.
- [45] G. Zhang, H. Zheng, Z. Hao, Z. Li, *Chem. J. Chin. U.* 37 (2016) 1380–1389.
- [46] J.P. Espinós, J. Morales, A. Barranco, A. Caballero, J.P. Holgado, A.R. González-Elipe, *J. Phys. Chem. B* 106 (2002) 6921–6929.
- [47] J.J. Teo, Y. Chang, H.C. Zeng, *Langmuir* 22 (2006) 7369–7377.
- [48] K.-H. Chuang, C.-Y. Lu, M.-Y. Wey, Y.-N. Huang, *Appl. Catal. A Gen.* 397 (2011) 234–240.
- [49] M. Trépanier, A. Tavasoli, A.K. Dalai, N. Abatzoglou, *Appl. Catal. A Gen.* 353 (2009) 193–202.
- [50] M. Davari, S. Karimi, A. Tavasoli, A. Karimi, *Appl. Catal. A Gen.* 485 (2014) 133–142.
- [51] J. Lu, L. Yang, B. Xu, Q. Wu, D. Zhang, S. Yuan, Y. Zhai, X. Wang, Y. Fan, Z. Hu, *ACS Catal.* 4 (2014) 613–621.
- [52] H. Li, J. Zhao, R. Shi, P. Hao, S. Liu, Z. Li, J. Ren, *Appl. Surf. Sci.* 436 (2018) 803–813.
- [53] J. Ren, P. Hao, W. Sun, R. Shi, S. Liu, *Chem. Eng. J.* 328 (2017) 673–682.
- [54] R. Shi, J. Zhao, S. Liu, W. Sun, H. Li, P. Hao, Z. Li, J. Ren, *Carbon* 130 (2018) 185–195.
- [55] J. Ren, W. Wang, D. Wang, Z. Zuo, J. Lin, Z. Li, *Appl. Catal. A Gen.* 472 (2014) 47–52.
- [56] L. Kang, J. Zhang, R. Zhang, L. Ling, B. Wang, *Mol. Catal.* 449 (2018) 38–48.
- [57] R. Zhang, L. Song, B. Wang, Z. Li, *J. Comput. Chem.* 33 (2012) 1101–1110.
- [58] X. Han, W. Sun, C. Zhao, R. Shi, X. Wang, S. Liu, Z. Li, J. Ren, *Mol. Catal.* 443 (2017) 1–13.
- [59] G. Prieto, M. Shakeri, K.P. de Jong, P.E. de Jongh, *ACS Nano* 8 (2014) 2522–2531.
- [60] Z. Wei, X. Li, J. Deng, J. Wang, H. Li, Y. Wang, *Mol. Catal.* 448 (2018) 100–107.